International Journal of Fatigue 155 (2022) 106617

Contents lists available at ScienceDirect

International Journal of Fatigue

journal homepage: www.elsevier.com/locate/ijfatigue

Investigation of fatigue damage growth and self-heating behaviour of cross-ply laminates using simulation-driven dynamic test

D. Di Maio [a,b,*], G. Voudouris [a], I.A. Sever [c]

[a] Mechanical Engineering Department, University of Bristol, UK
[b] Engineering Technology, University of Twente, The Netherlands
[c] Rolls-Royce plc, UK

ARTICLE INFO

Keywords:
Vibration fatigue
Composites
Damage growth
Self-heating
Simulation-driven dynamic testing

ABSTRACT

Structural integrity of aerospace assets is paramount for both the safety and economy of aviation industry. The introduction of composites into the design of aero-structures generated several economic benefits but also led to several challenges, including fatigue damage growth and self-heating behaviour. Fatigue of metals is widely managed by calculations of damage accumulation and prediction of residual life. These techniques do not always apply to the fatigue of composites, where the onset and propagation of damage are still under investigation. Furthermore, vibration-induced fatigue is even less understood because of a handful of failure criteria available and, also, because it is biased by the self-heating conditions of the material itself. The authors have underpinned one failure criterion for vibration fatigue and mapped that against self-heating and environmental temperatures. Despite the advances, several research questions were left open because of the complex multiphysics behaviour of fatigue which outreached the experimental capacity. Therefore, this research suggests a Simulation-Driven Dynamic Test (SDDT) framework that deconstructs vibration fatigue experiments into step-wise steady-state analyses. This novel approach will enable (a) investigating the failure mode mixity of the underlying failure criterion, and (b) simulating the surface temperature during the delamination growth under vibration conditions.

1. Introduction

The scientific community has been researching fatigue behaviour of composites materials for many years, and a recent review [1] highlights all the significant outcomes of those researches. Interestingly, most of the research community is focused on mechanical testing, which spans from low-cycle fatigue (LCF) to high-cycle fatigue (HCF) using different stress ratios. Vibration fatigue is not commonly investigated because of the self-heating behaviour occurring in visco-elastic materials, which makes the material behaviour time–temperature dependent. Therefore, it is preferable to test and investigate material fatigue without the influence of self-heating. The effects of both frequency and temperature require additional tests for calculating shift factor(s), which project the material performances to different time–temperature conditions. Nobody can argue about the lengthy process required for characterising composite materials.

The self-heating behaviour of materials is an area of investigation which is not only limited to composites, but also to other types of materials subjected to fatigue as reported in [2] and [3]. The former investigates the procedure of measuring small quantities of heat generated during the early loading cycles of the metallic sample because of its visco-elastic conditions. The latter reports the intrinsic dissipation due to self-heating effect in high-cycle metal fatigue. Both examples report on mechanical tests and models simulated under quasi-static conditions. The effects of self-heating behaviour are, however, less aggravating than the ones observed in visco-elastic materials as composites, for which some investigations are reported in the following papers [4-10] and [11]. All those researches are based on mechanical testing conducted at rates generating self-heating. They all indicate how that behaviour is highly detrimental to the residual life of the composites. The reader is highly encouraged to look at these papers before approaching the self-heating behaviour caused by vibrations.

Interestingly, papers [12,13] and [14] discuss the frictional heat developed at the crack tip interface in combination of the material self-heating. The studies are still focused on mechanical testing rather than harmonic or vibration responses. A model of self-heating [15] is proposed for the harmonic response which show how the self-heating of the material changes the system dynamics. Katunin et al. [16-30] have

* Corresponding author at: Engineering Technology, University of Twente, The Netherlands.
E-mail address: d.dimaio@utwente.nl (D. Di Maio).

https://doi.org/10.1016/j.ijfatigue.2021.106617
Received 22 June 2021; Received in revised form 20 September 2021; Accepted 18 October 2021
Available online 22 October 2021

extensively studied the problem of self-heating in composites under vibration conditions. The research outputs lead to evaluate fatigue limits based on the self-heating properties, and some of those properties were exploited for Structural Health Monitoring. Shou et al. in [31] proposes research about self-heating of composite particulate, which is investigated by means of vibration loading.

The past researches highlighted that the self-heating greatly depletes the material resilience under HCF. One can read that vibrations and self-heating can be advantageously when used for Structural Health Monitoring and Non-Destructive Evaluation. However, none of those papers indicated how vibration fatigue tests should be carried out to observe the (i) self-heating, (ii) the onset of delamination and (iii) the frictional heat developed at the delamination tip in the context of aerospace engineering, which needs to design structures capable of enduring integrity under many loading conditions. High Cycle Fatigue is one of those conditions. Therefore, vibration fatigue testing is a common standard for qualifying components more rapidly than mechanical testing. Unfortunately, vibrations and self-heating are coupled and so one cannot understand which one triggers a fatigue damage first; the mechanical of thermal forces?

To underpin some fundamental criteria enabling the use of accelerated fatigue tests, Di Maio et al. [32,33], Magi et al. [34,35] and Voudouris et al. [36] explored how the vibrations could be exploited for investigating the fatigue damage growth behaviour of the composite components made of IM7/8552. The major innovations achieved by those researches are briefly summarised as follows.

Magi exploited the advantages of vibration testing to explore the fatigue behaviour of tapered composite components [34]. Such a choice was driven by the engineering application focused on fatigue of composites fan blades. The HCF standard was, and still is, based on resonance frequency tracking which relates the resonance frequency changes to the stiffness degradation of the test article. That works for metallic components, but it was found to be very ineffective for composites. The paper proposed a way of tracking the vibration phase change over the number of excitation cycles, as it was noticed that the relative phase shift between the input excitation and the output response is proportional to the onset of delamination. The response phase tracking showed to be sixty times more sensitive than resonance frequency change. The vibration test required to keep the vibration amplitude constant, the excitation frequency fixed and to measure the phase shift (IN-OUT) throughout the fatigue test. The vibration test data showed a sudden discontinuity present in the phase trace and that was observed as delamination through microscopic measurements. However, only the follow-up paper [35] showed by numerical analysis some insights on the delamination growth and the change of response phase. That phase discontinuity was called “Critical Event” and was used as the failure criterion for terminating fatigue tests. The follow-up numerical investigation [35] evaluated the response phase (Fig. 1) and the crack growth (Fig. 2) as functions of cycles calculated by the Virtual Crack Closure Technique (VCCT). The phase decays linearly (see Fig. 1) because of the delamination growth (see Fig. 2) and the phase shift discontinuity was due to the increase of delamination rate. That work underpinned two aspects that experimental investigation could not resolve. First, the vibration response phase, which is monitored during the HCF testing, starts decreasing as soon as the delamination opens. Second, the Strain Energy Release Rate increases very rapidly when the response phase shows an abrupt change of decay rate.

What is that sudden discontinuity observed in the response phase curve? Both papers [33] and [34] did not investigate the physical forces generated at the crack tip and leading to that discontinuity, called Critical Event. Furthermore, those two papers did not investigate the effect of self-heating, the environmental conditions and their effects on the formation and propagation of the onset of delamination. The numerical investigation that will be presented in the following chapters will discuss the response phase (Fig. 1) behaviour during HCF and it will shed light on the damage mechanisms that drive these events (Fig. 2).

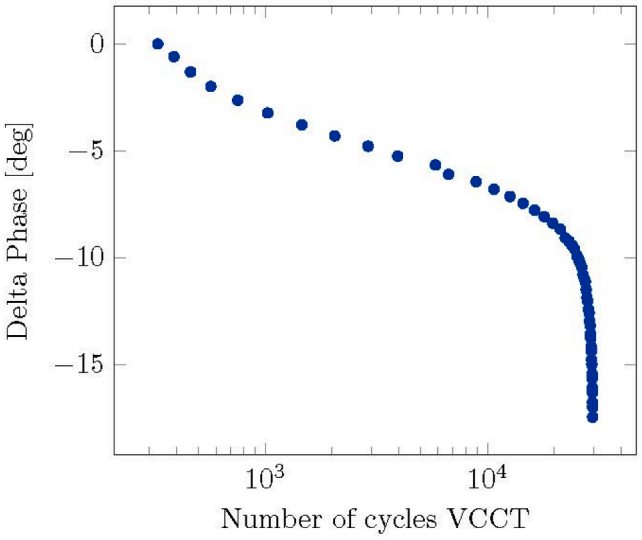

Fig. 1. Numerically generated vibration phase shift by VCCT method [35].

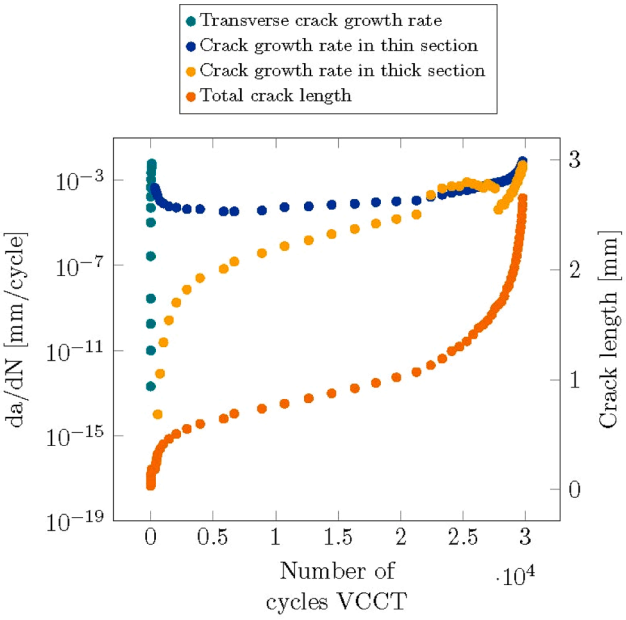

Fig. 2. Crack growth analysis by VCCT method [35].

Voudouris [36] exploited the same experimental technique and successfully captured the fatigue behaviour of composites while also considering elevated ambient temperature conditions. As a matter of example, Fig. 3 shows the vibration response phase with the Critical Event appearing at about 1.6 10^6 cycles as a sudden discontinuity (kink) likewise the surface temperature profile showing a hot-spot at the same number of cycles. Observations about self-heating were also addressed by Ruzek et al. in [11], who investigated the effects of loading frequency (0.5 Hz to 15 Hz) on the fatigue behaviour, the failure mechanisms and the self–heating temperature of tapered CFRP specimens. They observed a rapid increase in the surface temperature of the specimens due to the increased damage size. However, they reported no relation between the self-heating temperature and the fatigue life before this phenomenon. In other words, the authors considered the relation between the mechanical and thermal responses of composite components under cyclic loading during the testing stage where damage has not yet developed, or it was not large enough to affect the self-heating temperature. Voudouris et al. [36] also showed through a series of interrupted HCF tests and CT

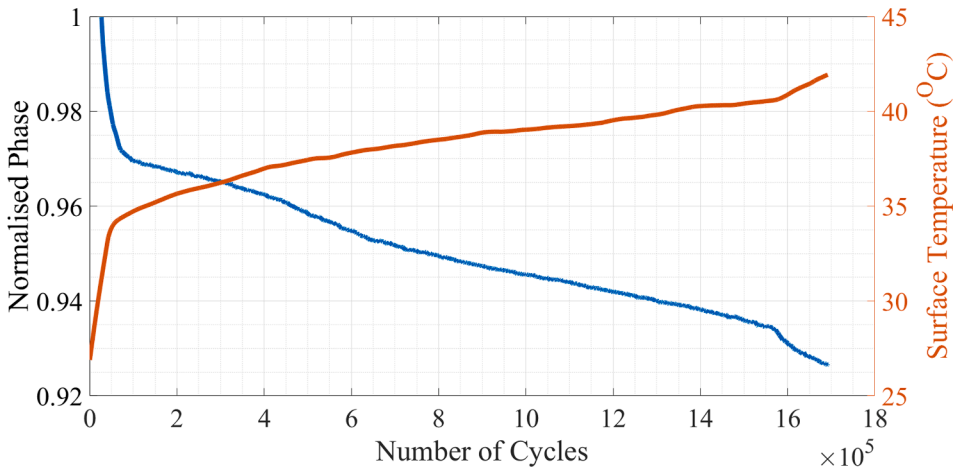

Fig. 3. Scaled vibration response phase (blue) and surface temperature (red) [36].

scan measurements how the delamination growth relates to the vibration response phase linear decrement over a number of cycles.

As briefly introduced earlier, Magi et al. [34,35] and Voudouris et al. [36] did not fully address the following topics which are listed hereafter, and they form the scientific contribution of this paper.

1. Calculate the failure mode mixity throughout the fatigue test. Compare the mode mixity behaviour with the response phase. Characterize the failure criterion identified as "Critical-Event", which is measured as a sudden change of slope in the vibration response phase over the cycles and which was not addressed in [35].
2. Verify by numerical simulation the temperature dependence of the "Critical-Event" observed during the experiments under different environmental temperatures, such as between 25 ℃ and 75 ℃, not proven in [36].
3. Calculate by numerical simulation the self-heating temperature over the number of excitation cycles, as shown in Fig. 3, and not done before for vibration fatigue.
4. Compare the experimental and numerical relationships "response phase-temperature self-heating" at various environmental temperatures, which is a novel outcome of this research.

Objectives 1) and 2) are presented in "mechanical response and results" section, objective 3) is presented in the "heat-transfer analysis and results" section and objective 4) is presented in "mechanical and thermal response results".

This paper aims at deconstructing complex vibration fatigue experiments into a series of steady-state dynamic and static analyses. This step-wise approach overcome limitations, such as time consuming transient analysis, during the numerical analysis and also enables tackling nonlinear interface behaviour that appears at the crack tip of the delamination. It will also provide some helpful guidance to designers on how to approach self-heating from a modelling viewpoint.

2. Finite element methods

The research work is entirely developed by Finite Element (FE) methods carried out by ABAQUS software with the aid of MATLAB scripts for the VCCT calculations. The following sections will describe the simulation methods used to achieve results that are referenced against test data that are already published in [36].

2.1. FE model and material properties

The first step towards simulating the fatigue life behaviour into a FE environment is to reproduce the dynamic testing environment. The testing coupons are restrained by a steel fixture that is attached to an electromagnetic (EM) shaker, a test set-up already presented in [34,36]. The EM shaker provides a base excitation, the acceleration of which is measured by an accelerometer. In terms of FE modelling, the fixture and shaker's armature are simulated with a non-structural mass located within the contact region of the two rods of the fixture (Fig. 4). A non-structural mass of 15 kg was added in the location of the fixture, and such a modelling approach is sufficient to take into account the lower resonant first bending frequency physically measured on the specimen.

The tapering, such as thickness reduction, is a widely used designing feature in various composite structures (e.g. fan blade roots) to achieve the desired geometry. These regions of discontinued geometric locations are achieved by dropped plies, giving rise to high interlaminar stresses [37]. In these scenarios, the load is transferred from the dropped plies to the resin pocket. Then, it is extended to the adjacent plies, forming a delaminated region. As Khan explained it in [37], the delaminations are driven towards the thin section of the laminate, only for steep thickness reduction. However, delaminations most commonly occur towards the thick section due to the high shear stresses. An FE approach is usually applied to simulate the delamination propagation within the damaged areas due to the complex physics governing the fatigue life of tapered laminates. Therefore, it is considered crucial to capture the effects of stress-raising features, like ply drops, when examining the failure mechanism of tapered laminates as their absence from the analysis could overestimate the components' capabilities. While on an industrial scale the simulation of tapered components, such as wind turbine blades [38], call for a homogeneous approach, on a smaller scale, a ply-boundary modelling approach can be considered. Therefore, another crucial aspect in the model development is capturing the actual shape of the ply drop region for a more accurate representation of both the dynamic response and the internal forces that can be achieved. For this reason, a CFRP specimen was cut and polished around the ply drop. Its micrograph (Fig. 5) was then used as a reference for simulating the specimen in the FE environment.

Two FE models were created. One as a 2D model for the mechanical analysis, as shown in Fig. 5 (bottom), and, one as a 3D model for the heat-transfer analysis. All dynamic simulations were carried out via steady-state analysis, even for the heat transfer, by a process described in the following flowchart diagram as shown in Fig. 6. The element types are presented in Table 1.

The Erdogan-Paris law parameters presented some unexpected challenges during the research execution. Unfortunately, only a limited amount of information was available in the literature regarding the Paris law parameters of the material used during the experimental investigation (IM7 /8552); especially, when exposed to various environmental temperatures. These material properties were not all available at the

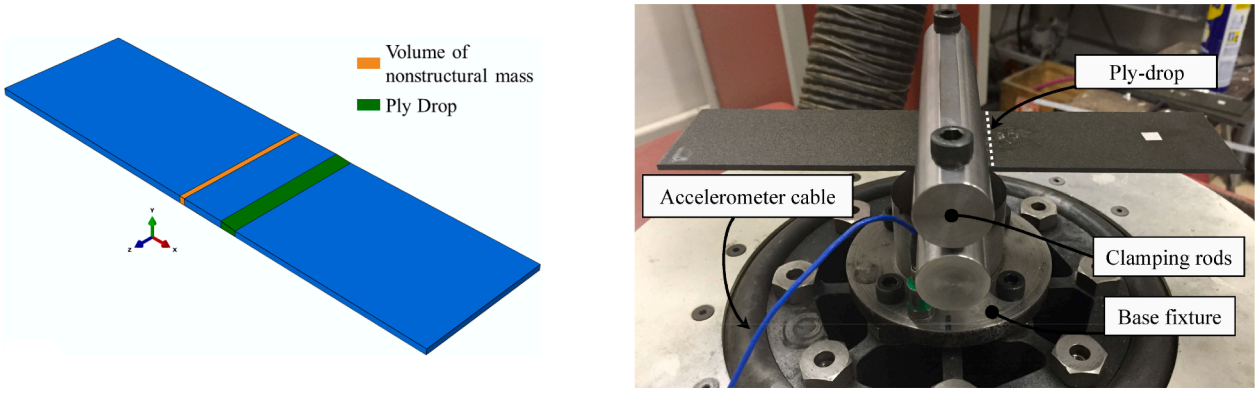

Fig. 4. The 3D geometry of a component on the left and component mounted in the fixture on the right.

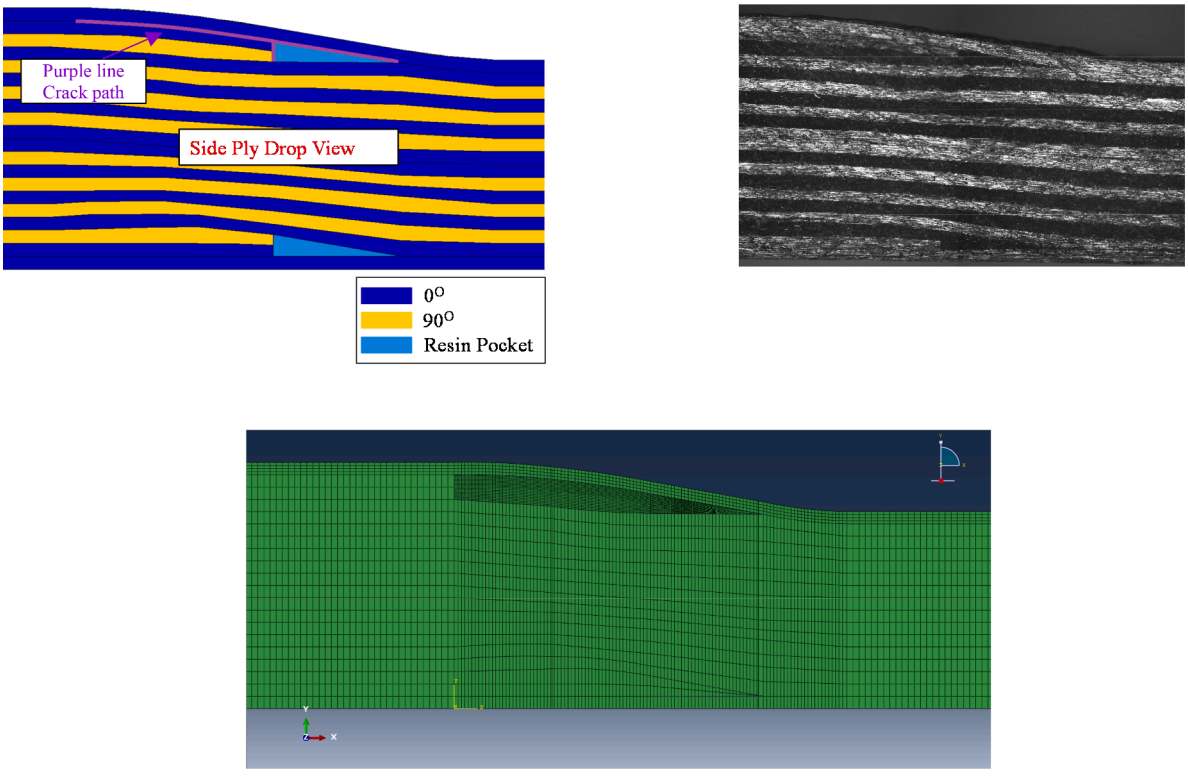

Fig. 5. Left – FE ply drop geometry / Right – Micrograph employed to partition the FE model, bottom-zoom of the mesh in the ply-drop region.

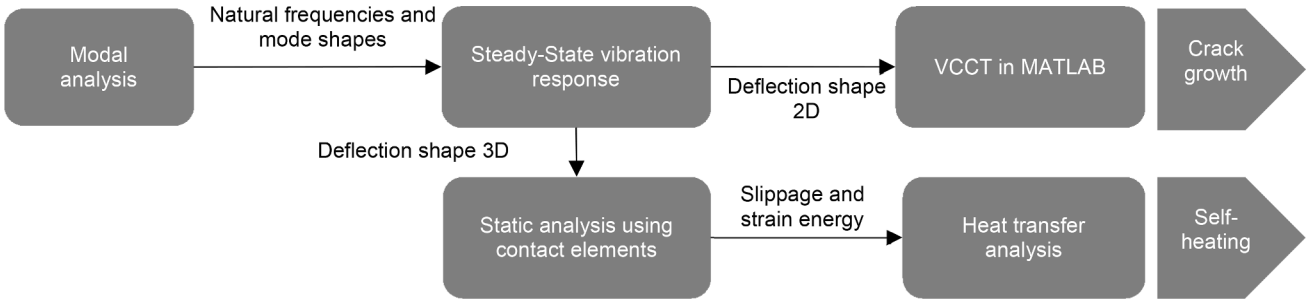

Fig. 6. Flowchart diagram of analysis carried out by the FE solvers and outputs.

time of the research (also out of scope) and, for this reason, it was decided to use a different CFRP material for the purpose of the numerical analyses. Hence, the studies carried out by Asp [39] and Sjorgen [40,41] were followed. The authors studied the Paris law parameters for a carbon / epoxy system, namely Hexcel HTA / 6376, at two environmental temperature levels (20 ℃ and 100 ℃). Moreover, for the purpose of the current study, an approximation was made in order to interpolate the results for an intermediate temperature level, at 60 ℃. Authors

Table 1
Element types used in the FE for the calculations.

VCCT Dynamic Element type CPS4 4-node bilinear Plane stress elements	Self-Heating Dynamic C3D8R Eight-node brick element with reduced integration
Self-Heating Thermal DCC3D8	Hot Spot Thermal DCC3D8 Forced convection/diffusion elements 8-node

might expect some scepticism from the readers about this choice, but the simulated results show that the choice did not make a noticeable difference. Hence, Tables 2-6 present the material and fracture properties of HTA / 6376, at three ambient temperature levels.

2.2. The Virtual crack Closure technique (VCCT)

It is widely known that the VCCT is commonly applied in order to provide information about the crack growth rate. Hence, it is possible to utilise this technique to simulate the occurrence of the Critical-Event at various ambient temperature conditions. The purple line of Fig. 5(left) depicts how the crack propagates under cyclic loading, which was also reported in [34,36]. However, presents more accurate data from the interrupted tests and CT scan measurments which were combined with the VCCT for the development of the simulations. Interrupted tests demonstrated that the crack would emerge as a transverse crack between the terminated plies and the resin pocket. Therefore, it is safe to assume that the damage will initiate where the resin pocket meets the transverse ply since the stress concentration at this region is the highest; then, it will propagate towards the outer ply [37]. The CT scan analysis of the interrupted tests showed that as soon as the transverse crack reaches the outer ply, the crack extends towards the thicker section of the ply drop, and then it extends towards both the thin and the thick sections, forming a "T" as shown in Fig. 7. The VCCT simulations also confirmed the propagation rate and direction.

2.2.1. The Erdogan-Paris law

The VCCT dictates that a crack will extend towards the direction that the total energy released, G_T, exceeds the fracture toughness, G_C, of the actual mode mixity G_{II} / G_T. Therefore, its main objective is to calculate the Strain Energy Release Rate (SERR) in order to estimate whether a major delamination will occur. After the initiation of the delamination, propagation follows the Paris Law while the crack growth rate depends on the relation between the G_T and G_C. Thus, the crack accelerates when the total energy available is close to the critical fracture toughness.

Russell and Street used an approach based in Fracture Mechanics and proposed that the Paris law between pure mode I and pure mode II can employed utilising a simple rule of mixture [42].

$$\frac{da}{dN} = C_m\left(\frac{\Delta G_I}{G_{Ic}} + \frac{\Delta G_{II}}{G_{IIc}}\right)^{n_m} \tag{1}$$

Where C_m and n_m are the Paris law parameters, G_I and G_{II} are the SERRs for mode I and mode II while G_{Ic} and G_{IIc} are the critical SERRs.

$$C_m = \frac{G_I}{G_T}C_I + \frac{G_{II}}{G_T}C_{II} \tag{2}$$

$$n_m = \frac{G_I}{G_T}n_I + \frac{G_{II}}{G_T}n_{II} \tag{3}$$

The crack experiences different R – ratios for mode I and mode II during a complete oscillation. Magi [35] pointed out that R = – 1 at mode II while R = 0 at mode I, even though reverse loading exists due to the resonance vibration. Furthermore, Matsubara et al. [43] argued that the ΔG_{II} definition lacks physical meaning. For this reason, they introduced the following relation which depends on the load range ΔP:

$$\Delta G_{II} = \Delta P^2 \hat{A}\cdot\left(\frac{G_{II}}{P^2}\right) \tag{4}$$

$$= P_{max}^2 \hat{A}\cdot(1-R)^2 \hat{A}\cdot\left(\frac{G_{II}}{P^2}\right) \tag{5}$$

$$= G_{IImax}\hat{A}\cdot(1-R)^2 \tag{6}$$

Taking into account Eq. (6), the Paris law in Eq. (1) can be transformed into:

$$\frac{da}{dN} = C_m\left(\frac{G_{Imax}}{G_{Ic}} + \frac{4G_{IImax}}{G_{IIc}}\right)^{n_m} \tag{7}$$

As a result, the crack propagation rate $\frac{da}{dN}$ can be calculated for both crack tips of the "T" shape, using an iterative process in an FE environment, but it will only propagate towards the region where G_T is higher. The number of cycles can then be estimated for each iteration, by subtracting the life of the failed element by the residual life of the adjacent element sharing the crack. However, it is worth noting that the crack propagation rate was already investigated in [35] and therefore in not repeated in here.

3. Investigation on vibration-driven delamination growth

The major difference provided by this paper with the state-of-the-art VCCT simulations is that components are subjected to vibration loading and environmental temperature. The simulation process requires three-step calculations that are the following: modal analysis, steady-state (s-s) dynamic analysis and VCCT calculations. Furthermore, ABAQUS solver and MATLAB are coupled for the s-s analysis because the deflection shape calculation is always carried out for a constant strain amplitude. This means that once a node is open, because of the VCCT calculations, a new deflection shape must be calculated meeting the constant strain amplitude at the target measurement location. The VCCT calculations to grow delamination are carried out in MATLAB, which uses the modal deflection shape as a static loading condition. Therefore, similar to the experiments, the strain of the VCCT models was calculated at a fixed point (element on the model) while different loads were applied in order to examine the system's behaviour at different severity levels. The measurement point of the simulated strain coincided with the point at which the strain was measured during the experimental investigation.

Even though the damage between the different instances (e.g. resin pocket, plies) was pre-imposed on the FE model, massless springs were applied at each node of the contact region between the instances, all along the crack path, in order to maintain the crack closed for as long as it is required. So, the damage is propagated by removing the appropriate springs during one iteration of VCCT in MATLAB. Only two springs were applied at each node, corresponding to the two axes of the 2D model. The springs are crucial for the VCCT analysis since they permit the extraction of nodal forces, which the VCCT calculations can then exploit. As already hinted at, the modal deflection shape for given excitation frequency and strain load is calculated by steady-state dynamics in ABAQUS, then the max and min modal displacements are used as a static loads for calculating the SERR of both failure mode-I and -II while the springs at the onset of damage were removed. Additionally, the spring stiffness was chosen in order to promote a rigid bond between the contact areas, at a magnitude six times greater than the rigidity of the corresponding 0° ply. This approach ABAQUS-MATLAB does not take into account the friction forces between the delaminated plies; it is

Table 2
Physical and Mechanical Properties of HTA/6376 [39,41].

E_1 (GPa)	$E_2 = E_3$ (GPa)	$\upsilon_{12} = \upsilon_{13}$	υ_{23}	$G_{12} = G_{13}$ (GPa)	G_{23} (GPa)	ρ (kg/m^3)
120	10.5	0.3	0.51	5.2	3.4	1586

Table 3
Fracture mechanics properties of HTA/6376 [39,41].

	20 °C			60 °C			100 °C		
	G_C (J/m^2)	C	n	G_C (J/m^2)	C	n	G_C (J/m^2)	C	n
Mode I	260	1.2×10^{-7}	5.5	255	2.2×10^{-6}	4.9	249	4.2×10^{-6}	4.2
Mode II	1002	7.5×10^{-7}	4.4	852	8.3×10^{-7}	4.5	701	9.1×10^{-7}	4.6

Table 4
Physical, Mechanical & Thermal Properties of epoxy resin 8552

E (GPa)	υ	ρ (kg/m^3)	κ (W/m°C)	C_P (J/kg°C)
5	0.3	1310	0.35	1000

Table 5
Thermal Properties of UD laminate IM7/8552.

κ_1 (W/m°C)	$\kappa_2 = \kappa_3$ (W/m°C)	C_P (J/kg°C)	h (W/m^2°C)
5.4	0.95	857	10 – 80

Table 6
Dynamic Parameters.

Structural Damping	Frequency [Hz]	Non – Structural Mass [kg]
0.0035	395	15

assumed negligible until the critical delamination size.

Fig. 8 illustrates a comparison between the experimental and simulated data of the vibration phase for three strain levels. The discrepancy between experimental and simulated results is mainly attributed to the 2D prismatic geometry of the VCCT models and the use of different material properties between the physical and model components. Despite that, the simulated data seem to show a good degree of agreement with their experimental counterparts. Additionally, one can notice that the phase evolution of numerical results mimics the observed behaviour, as it goes from a low to a high number of cycles. Nevertheless, the VCCT analysis reports a slightly higher fatigue life with increasing strain while outlining different deterioration rates (slopes) in the respective region of the phase evolution. On top of that, it was also able to simulate the fatigue life at severity levels attempted during the experiments. One major difference in here is the use of strain as reference level instead of the displacement as used in [35].

3.1. Buckling of the delaminated plies at the critical event

Magi et al. [35] performed the VCCT analysis, but the authors did not explain why the strain energy release rate increased rapidly at the so-called Critical-Event. The interrupted tests and CT scan measurements in [36] provide helpful insight into appearance of the Critical-Event. However, both papers do not clarify what drives the delamination growth rate to build so rapidly.

Before investigating the forces behind the appearance of the Critical-Event, Fig. 9 illustrates how the VCCT technique can be employed to simulate and study the influence of increasing severity; at the same ambient temperature level. The data collected from the simulation were employed to create a typical double logarithmic graph of damage growth rate against the Energy Release Rate (ERR). The ERR was

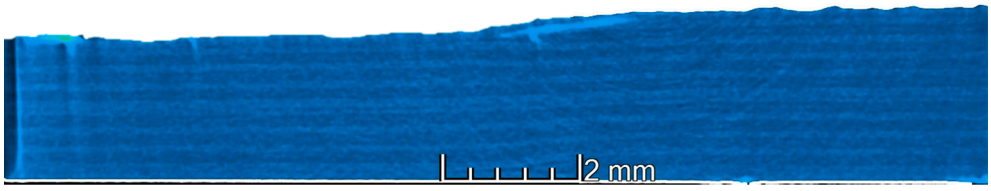

Fig. 7. Example of CT scan from [36].

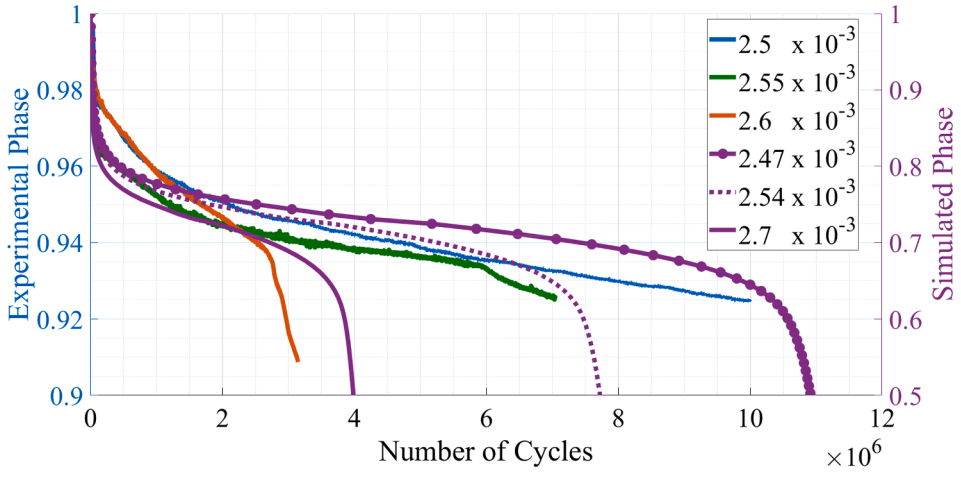

Fig. 8. Comparison between Experimental and Simulated Phase evolutions at different severities and at 25 °C.

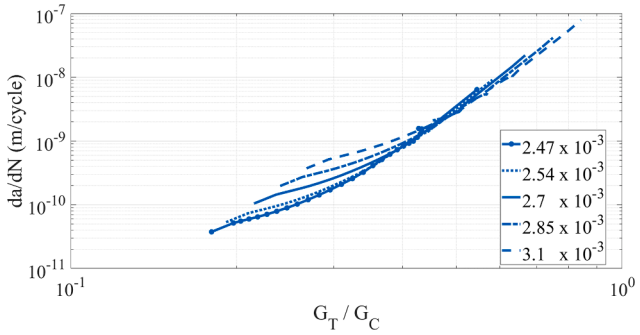

Fig. 9. Comparison of the simulated crack growth rates at different loading severities.

normalised against the fracture toughness (G_C) to eliminate any variations caused by G_C.

Furthermore, Fig. 9 implies that the crack growth is slower in the initial stages of endurance testing, corresponding to a lower ERR. However, the damage growth accelerates under the effect of higher ERR, reaching a threshold limit. It is apparent that the severity will not affect the crack growth significantly during vibration testing. This can be attributed to the fact that the threshold values are identical for the tests performed at the same ambient temperature since the strain dependency is more evident at lower ERRs. In other words, the difference between the fracture toughness and the total strain energy is smaller under the effect of higher strain, resulting in rapid damage development.

The previous paragraph suggests that for any strain load, the delamination growth would not change. Similar to both the information available in the literature and the experimental observations captured by the X-ray Computed Tomography in [36], the FE results show that the delamination will first propagate towards the thick side of the ply drop and then towards both the thick and the thin sides (Fig. 10). This is considered an initial indication that the VCCT model can simulate the damage growth pattern sufficiently due to vibrations. The mode mixity ratio $\frac{G_{II}}{G_T}$ was calculated over the number of vibration cycles to evaluate the failure mode at the critical event.

Fig. 11 presents the typical response phase and mode mixity at the crack tip of a composite laminate during the vibration fatigue life, as simulated by VCCT. It is apparent that the mode mixity ratio goes nearly to null, and so the Critical Event is mainly dominated by failure mode-I. In other words, the delamination reaches a length which buckles because of the compressive forces generated at either ends of the delamination during one half cycle of the vibration, similar behaviour reported in [44]. This result seems plausible and thus explaining why the vibration response phase decreases so rapidly. There is a moment during the fatigue life when the buckling conditions enable the crack to propagate very rapidly, and so the response phase (proportional to the stiffness) decays very abruptly. Bolotin [44] reported that delamination buckling is typically seen in surface ply delamination. Magi et al. [34] showed experimintal results of a scaled-model of fan blade subjected to fatigue where some delaminations appear in the core of the blade root. It might be very possible the the response phase tracking is much more sensitive than other measurement parameters observed during mechanical testing.

Further analysis of the VCCT results showed that the phase drop is linearly proportional to the damage size. Table 7 presents how the response phase correlates to the crack opening at two different instants

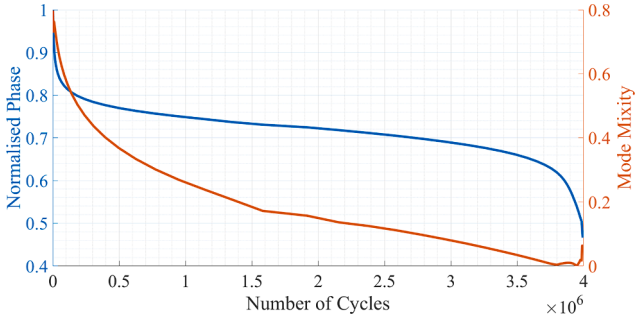

Fig. 11. Typical Phase and Mode Mixity as captured by VCCT.

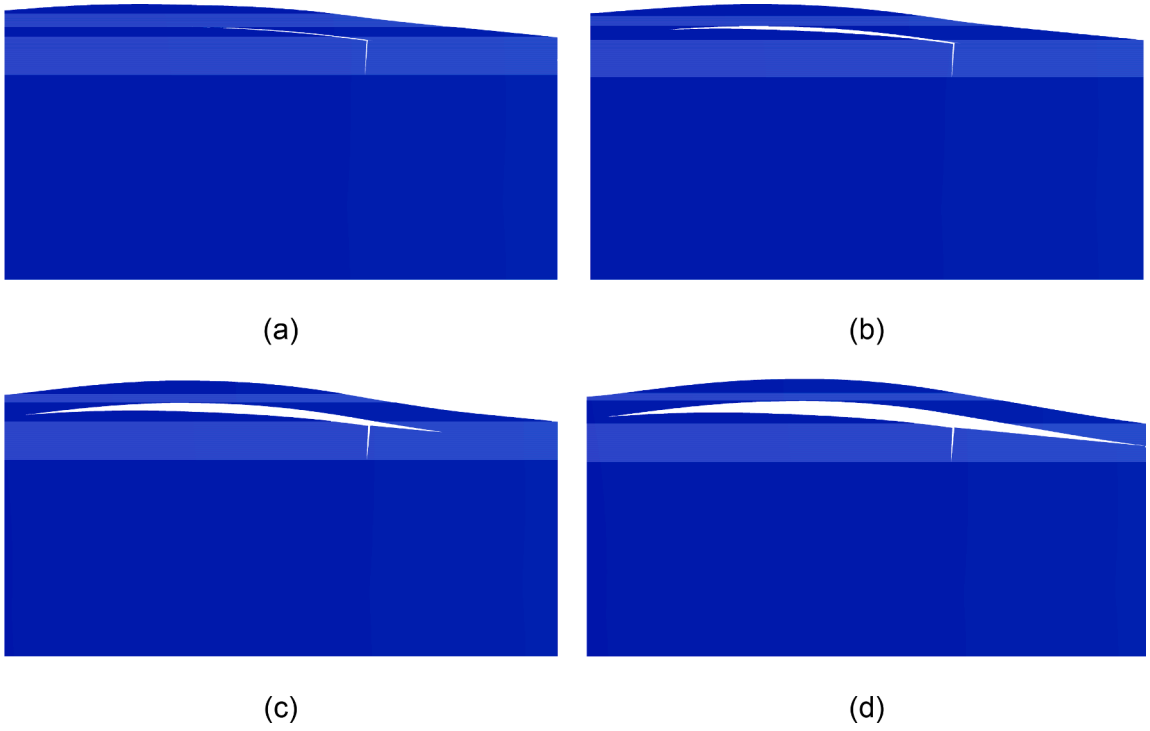

Fig. 10. Typical Damage Evolution as captured by VCCT.

Table 7
Comparison between the Damage Area and Phase decay for two strain levels, as captured by VCCT

	At Point A			At Critical Event		
Load Severity	Number of Cycles	Scaled Phase	Delaminated length (mm)	Number of Cycles	Scaled Phase	Delaminated length (mm)
Low	7.88×10^5	0.78	0.694	10.2×10^6	0.64	1.426
High	3.08×10^5	0.78	0.695	3.71×10^6	0.64	1.424

of the fatigue life. The table indicates that regardless of the load severity Critical Event always occurs at the phase (scaled to unity) of 0.64. This value is case-dependent, specific to the component under test. Nevertheless, there might be a characteristic value associated to each layup configuration. As a final remark, that value is more challenging to be found by experiments as one should always start any test from the same phase reference, which in practice is difficult to achieve.

3.2. The effects of different environmental temperature levels

This section is about the use of VCCT models to analyse the vibration fatigue testing under different ambient temperature conditions. To achieve this, the properties of the material presented in Section 2.1 were used. The traces in Fig. 12 demonstrate a comparison between the experimental and simulated mechanical responses, as they are described by the decay in vibration phase, at different exposure temperature environments but at the same strain level (2.6×10^{-3} for the experimental data and 2.7×10^{-3} for the simulated). It is evident that the VCCT can reproduce the vibration fatigue life at different ambient temperatures.

Similarly to the numerical approach employed to simulate the fatigue life at different strain levels, Fig. 13 accommodates the fatigue damage growth rates at three different temperatures. In this case, the simulations were conducted at the same strain level. It can be noticed that the vibration fatigue data can form straight lines, which permits the application of a power fit; hence, it follows the Erdogan-Paris's equation. The traces chart similar patterns while presenting a considerably accelerated rate at 100 °C, compared to 20 °C. This behaviour illustrates that the specimens are significantly more prone to damage under harsher temperature environments since the energy required to open the crack at higher environmental temperatures is lower, as also reported in the literature.

Similarly, the simulated fatigue life curves at different ambient temperature and severity levels can be outlined. Fig. 14 contains the simulated S-N Curves for three different ambient temperatures and three different strain levels. As expected, both the environmental conditions and the strain levels imposed contribute to the degradation of composites when subjected to high frequency cycle vibration testing. It appears that the influence of the exposure temperature is less severe on the simulated curves when compared with the respective experimental curves. Interestingly, this S-N plot shows straight lines which are shifted because of the effect of the environmental temperature but it does not show any significant change of slope. The experimental results on the other hand showed a very clear change of slope as published in [36].

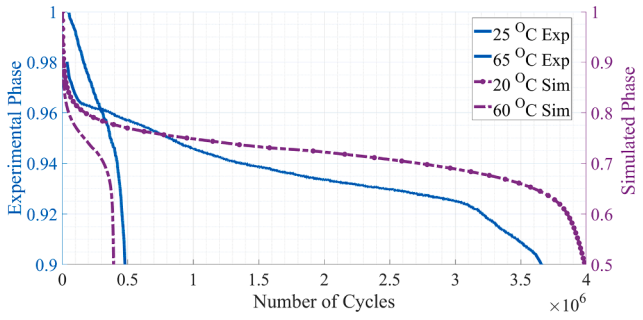

Fig. 12. Comparison between Experimental and Simulated Phase evolutions at different ambient temperature levels and at the same severity (2.7×10^{-3}).

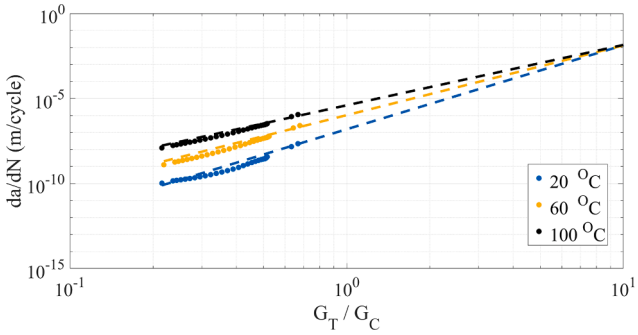

Fig. 13. Comparison of the simulated crack growth rates at different ambient temperature levels.

One possible explanation is that the simulation process undertaken in here does not include time-dependence of the self-heating behaviour associated with the material subjected to fatigue. In fact, the numerically generated S-N curves do not include the multiphysics behaviour of the material, but those plots describe how the residual life changes at certain given cycle steps, which were considered in the VCCT analyses. In reality, the material behaviour continuously changes throughout the fatigue during which the heat is continuously dissipated. This topic will be further explained in the next sections.

3.3. Crack growth propagation rate

During this investigation on the crack growth, it became clear that its growth can be directly correlated to the change of vibration response phase. Table 7 presents that the phase is strongly dependent on the damage size. Therefore, it is logical to assume that the vibration phase rate can be correlated to the crack growth rate. Unfortunately, the interrupted tests in [36] presented that correlation at one ambient temperature and for a single strain level.

The VCCT can be exploited in this sub-section to provide a better insight into the response phase-damage relationship. Fig. 15 compares the phase decay and the crack growth rate, as simulated for different ambient temperature and strain levels. It is clear that the response phase-damage relationship is not significantly affected by the surrounding temperature or the applied severity. In fact, Fig. 14 demonstrates a linear relation for all the cases that were studied. It is worth noting that linear forecasts were employed alongside the fitted lines to better compare the simulated results since higher severities and harsher environmental conditions could lead to accelerated crack growth rates. Hence, lower propagation rates could be too small to plot alongside the cases that yield rapid damage opening without forecasts. However, for completeness purposes, the actual simulated data are also presented in Fig. 15. Additionally, few outliers that are apparent on this figure correspond to the final steps of the fatigue life (after the Critical Event).

4. The thermal response analysis by multiphysics FE models

The previous section attempted to prove a failure mode describing the so-called Critical-Event and the effect of temperature on the appearance of such an event as a function of excitation cycles. The section showed that S-N curves could be created at different

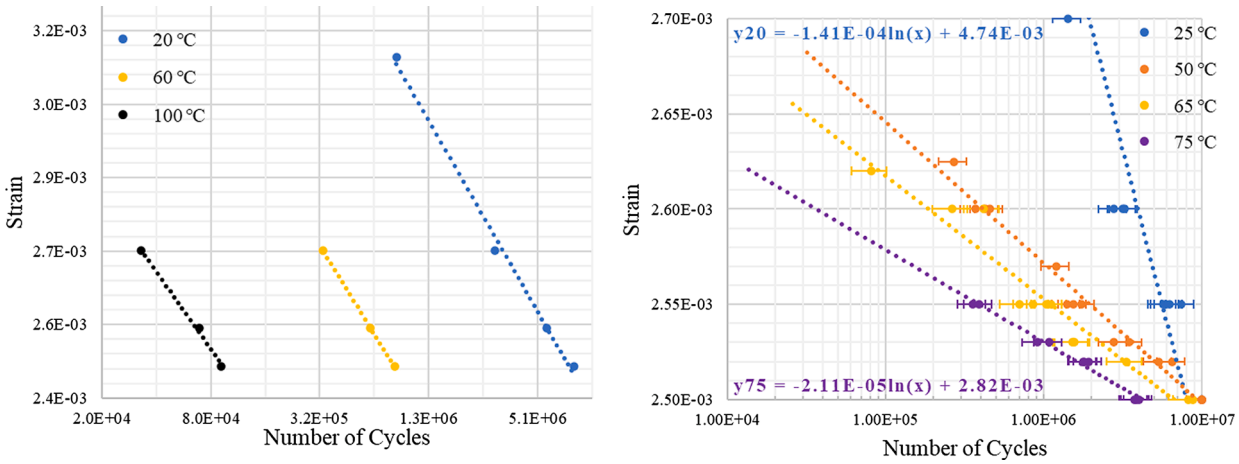

Fig. 14. Simulated (left) and measured [36] (right) fatigue life curve at different ambient temperatures.

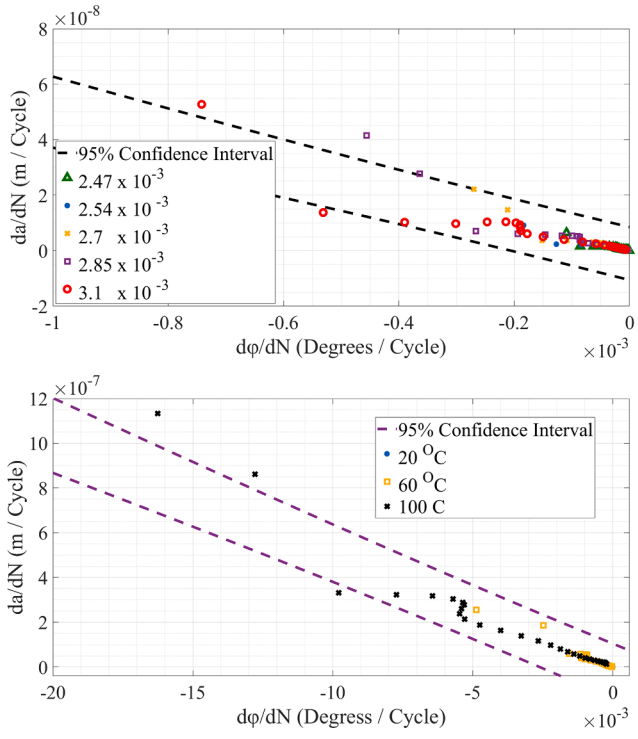

Fig. 15. Simulated Damage Growth Rate against Response Phase Decay / Top – Same ambient Temperature but different strain levels / Bottom – Different ambient Temperatures but same strain levels.

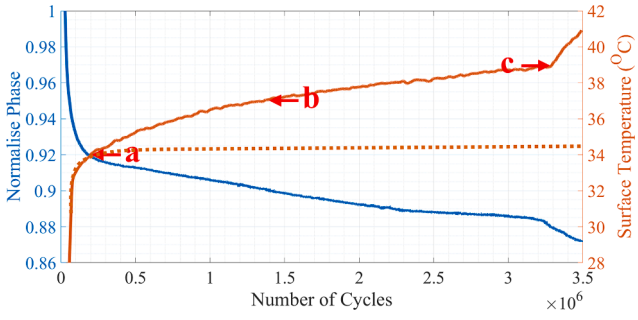

Fig. 16. Self-heating temperature during a vibration fatigue test.

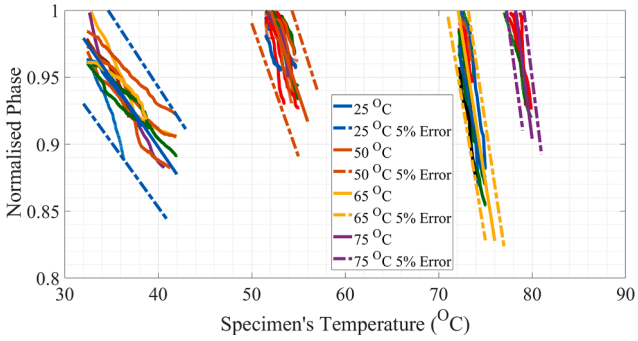

Fig. 17. Experimental relationships between response phase and self-heating temperature [36].

temperatures based on the Critical Event failure criterion, as shown in Fig. 14. The simulated S-N curves showed an offset in the number of cycles to failure dependent on the environmental temperature, but those simulations could not capture the varying slopes present in the experimental ones presented in [36], which we assume depending on the self-heating behaviour of the material. This section aims at including the self-heating behaviour into the fatigue life of the samples tested for this research. Fig. 16 shows typical relationships for the self-heating temperature and vibration response phase.

A new plot can be made by plotting those two curves as one against the other, as shown in Fig. 17 (reproduced from [36]). We wish to draw attention to the impact of self-heating and environmental temperatures on the Phase Vs Surface Temperature relationships.

Unlike what was discussed for the Virtual Crack Closure Technique, fewer references are available in the literature for the simulation of self-heating temperature and hot-spot temperature during vibration fatigue conditions. For this reason, a conservative approach was employed. The viscoelastic heating was established by estimating the system's elastic (modal) strain energy, while the hot-spot temperature was simulated separately by evaluating the frictional work on the damaged area. After that step, the energy generated was used as heat input to a heat transfer analysis. Various exposure temperatures can then be considered by applying different boundary conditions in the heat transfer analyses.

4.1. Self-heating modelling

The internal heat generated during a vibration fatigue test because of the material's visco-elastic properties is referred to as the "Self-Heating", and the temperature trace can be divided into three parts: A, B and C in Fig. 16. These three temperature areas resemble very much what is

observed in literature. However, one should notice that the last area (Region C) consists of a very small delamination area (approx. 5 mm × 5 mm), which is much smaller than the damage seen for mechanical testing.

Region A: the temperature is the equilibrium between the hysteretic heat the heat dissipation. That temperature would not change as a function of cycles without fatigue damage, as shown by the dashed line in Fig. 16.

Region B: the temperature is characterised by the increase of strain energy. The rate of increase is constant until the critical event when the delamination size is large enough to show a significant contribution of frictional heat.

Region C: the temperature is characterised by a sudden increase of localised temperature caused by frictional heat. The delamination size is large enough to yield local heat generation.

The temperature trace is the maximum one recorded from the heated sample surface, and therefore, temperature distribution over the whole surface of a specimen requires a 3D model and a heat-transfer analysis.

4.2. Self-heating of region A

Lahuerta et al. [45] described a method for simulating viscoelastic self-heating temperature of unidirectional laminated coupon under cyclic bending loads. They demonstrated that the viscoelastic heat of the components is related to the strain energy through a damping factor. It is, therefore, possible to develop a FE model which exploits this relation. In that respect, the strain energy can be extracted as follows. First, the deflection shape is simulated at steady - state conditions for a given strain load and then the resultant strain energy is then used as a heat input for the heat transfer analysis while always considering a damping factor.

An important part of the thermal model can be traced down to the thermal properties of the system since they can affect the final results. Even though Hexcel provides an extensive datasheet about the mechanical properties of the material system, its thermal properties are not studied as broadly. However, different sources present slightly different results [46-48]. As a consequence, a sensitivity analysis was conducted to identify the optimum values. The results expressed that with increasing conductivity, the endogenous temperature of a component decreases. However, the effects on the surface temperature are minor (<1℃) for the conductivity range of interest.

Moreover, the specimen's temperature is not limited solely to changes in the convection coefficients. It was observed that the airflow could drastically change the surface temperature distribution shape.

Fig. 18 demonstrates that increased convection could lead to changes in the temperature distribution shape, indicating that the modelled environment is not similar to the experimental conditions. The analysis of the thermal images showed that the heat convection is more significant at the edges of the specimens, resulting in an oval-shaped temperature distribution around the most stressed region (ply drop). This is another phenomenon that ought to be considered in the FE model in order to acquire a precise temperature distribution shape. A higher convection value was chosen around the model's edges to simulate the experimental observations accurately. On top of that, the ambient temperature can also be varied, which is a great advantage since the model could find application into various environmental temperatures levels. Fig. 19 shows a comparison between the real temperature and the simulated one, although the temperature scale might be confusing, the readings are very close. Fig. 20 shows a quantitative correlation between simulation and measurement results.

However, before moving to region B, we shall briefly discuss the region up to point A in Fig. 16. The experimental analysis illustrated how the equilibrium temperatures (point A, where no onset damage has occurred) of coupons are unaffected by the test's strain load severity as reported in [36]. Fig. 21 depicts the increase of the elastic strain energy of a specimen at the three different strain levels, which coincide with the severities of the VCCT models. While the strain energy is subjected to an increase of 14%, its effect over the maximum viscoelastic temperature is negligible, according to the experimental observations. It is, therefore, safe to assume that the strain range of interest is not sufficient to influence the viscoelastic temperature of specimens.

4.3. Self-heating of region B

The modelling of the self-heating of region B proved challenging. The interrupted tests, presented in [36], highlighted that the onset of delamination is already present but small in size to produce and significant frictional heat that the thermal camera could measure. The surface temperature was calculated by using the heat-transfer analysis, where the input energy load was the modal strain energy of one cycle of vibration (steady-state analysis). That simulated temperature was to be scaled by the number of excitation cycles, and that was achieved by information gathered from the five interrupted tests where both response phase and temperature curves were available. Thus, each of the

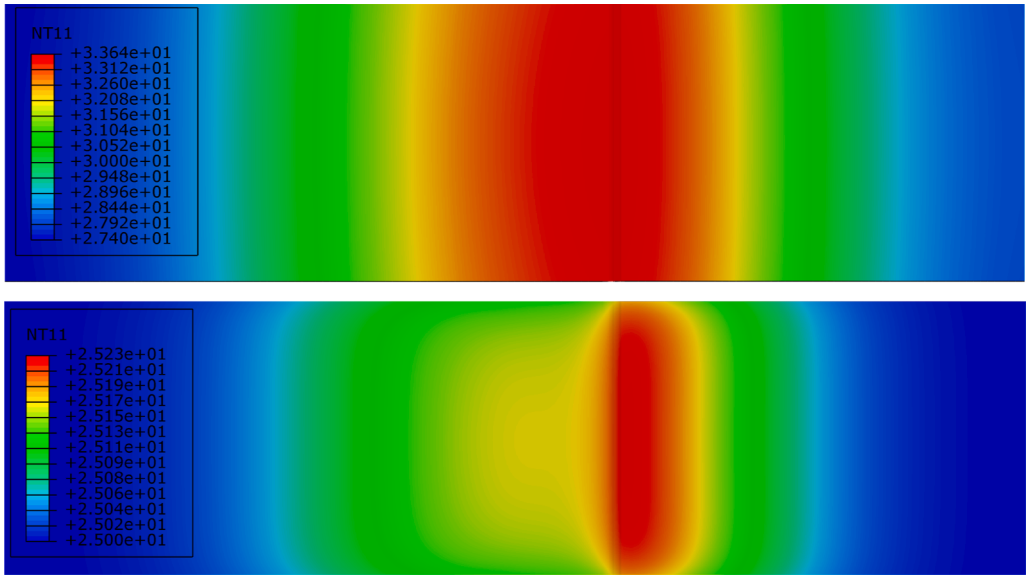

Fig. 18. Temperature distribution at Low (top) and High (bottom) Flow Rates in the FE environment.

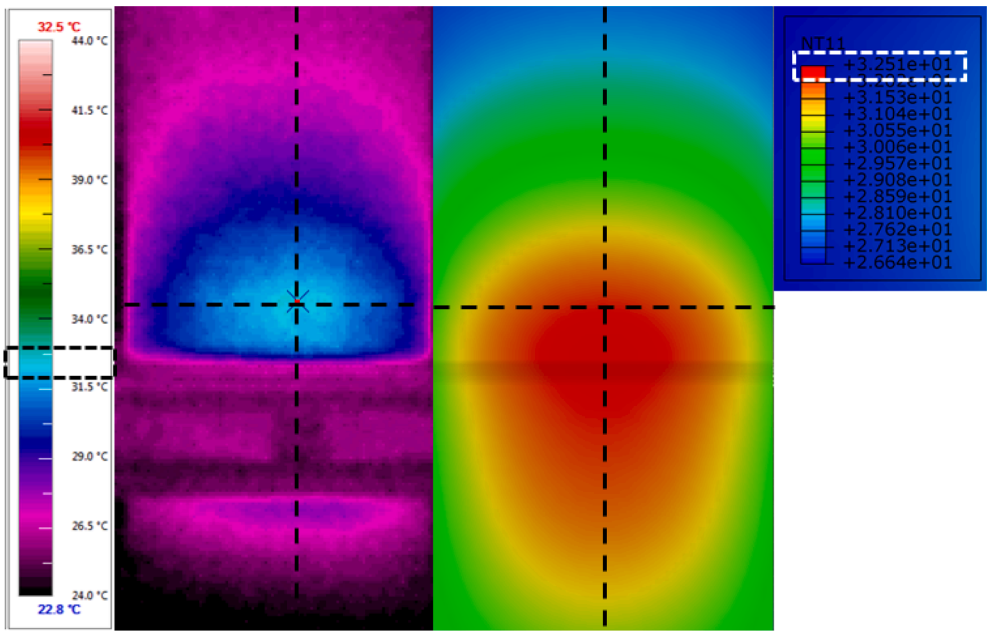

Fig. 19. Comparison between the experimental (left) and FE (right) temperature distributions along the surface of a specimen (black dashed lines refer to the correlation lines).

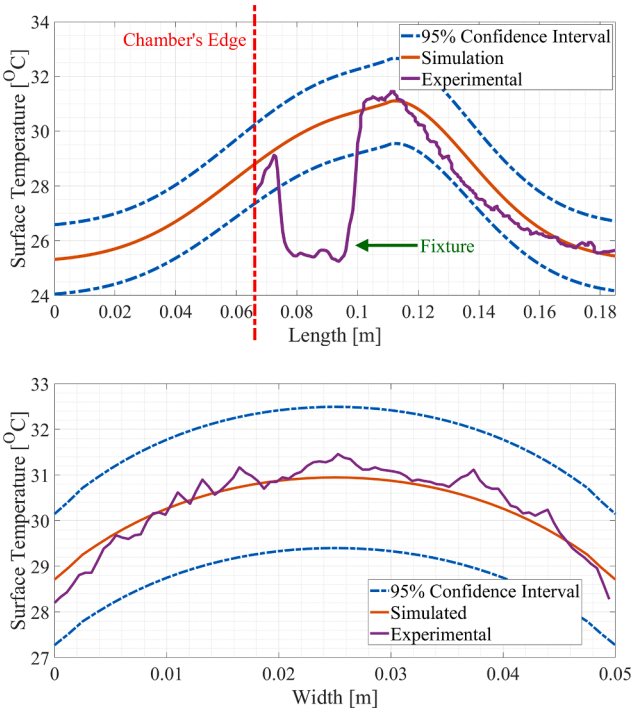

Fig. 20. Numerical comparison between the experimental and FE temperature distributions along the length (top) and width (bottom) of a specimen.

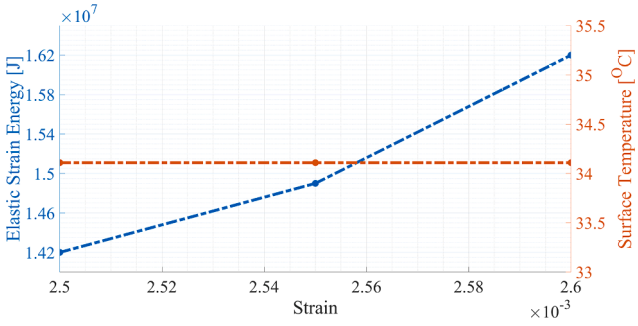

Fig. 21. The change in the Elastic Strain Energy and its respective viscoelastic Temperature due to the increase in the applied strain.

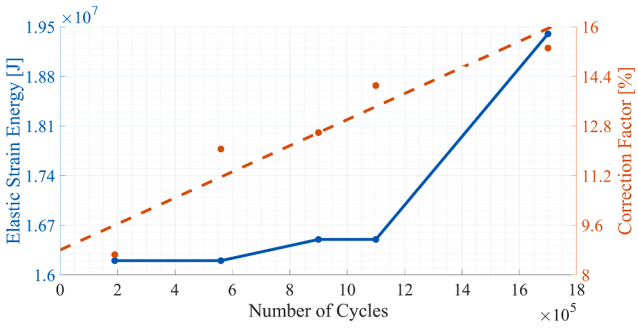

Fig. 22. The change in the Elastic Strain Energy and its respective Correction Factor due to damage propagation.

steps of Fig. 22 can be correlated to a different interrupted test since the delamination area was modelled as indicated by the CT scan images of the interrupted tests. The correction factor is a percentage between the surface temperature measured from the model for one cycle and the surface temperature measured for N cycles in the actual test. Therefore, the elastic strain energy for that vibration mode can be calculated according to the number of cycles. Fig. 22 displays the Elastic Strain Energy (fully reversible process) growth for the five models featuring different delamination sizes and the calibration function employed; at an ambient temperature of 25 °C. The number of cycles used in this figure corresponds to the number of cycles of the respective interrupted tests. This approach is empirical and aimed at these specific test cases. The process leading to an increase of elastic strain energy is simulated due to the damage growth over the five measured steps. Hence, an empirical mathematical model can be created, where CF is the Correction Factor and N the Number of cycles:

$$CF = 4.2*10^{-6}*N + 8.8 \quad (8)$$

4.4. Self-heating point C

This final section deals with the frictional heat generated by the delamination at and after the critical event. This final stage is the most challenging analysis, without any doubt, because friction is a non-linear phenomenon that cannot be calculated by steady-state dynamic analysis yet. The transient analysis was beyond the scope and the computational capacity available in this research. The heat developed due to ply-by-ply rubbing in the delaminated area is governed by the frictional contact forces. Friction is inherently a non-linear phenomenon, and linear steady-state dynamic steps cannot capture such behaviour. This target could be achieved by implementing a step-wise approach. The first step is to calculate the deflection shape under steady-state conditions, and this is done for every selected delamination size. The deflection shape is used as input boundary conditions in the static analysis where the interface of the delaminated plies can be modelled with contact elements (non-linear). Both the strain energy and the slippage at the delamination interface are calculated and become the input for the heat transfer analysis, such as the strain energy for the visco-elastic heat and the friction work yielded by the interface slippage for the frictional heating. Both thermal outputs are linearly summed. The delamination was pre-introduced in the model according to the observations made by the CT scans and their respective thermal images taken from [36]. The friction coefficient is an aspect of great importance for a multiphysics model. An experimental study carried out by Schön [49] on a CFRP material system (HTA / 6376), reported that the peak coefficient of friction falls within 0.7 and 0.8. Fortunately, it is possible to conduct a numerical sensitivity analysis within that range of coefficient in order to examine the effects of different friction coefficients on the friction generated temperature. In the end, both the maximum temperature recorded during the interrupted tests and the literature data were taken into account, concluding that the optimum value of the friction coefficient is close to 0.75. Hence, this value can be employed in the investigation of self-heating temperature of the specimen after the Critical Event. Fig. 23 shows an example of hot-spot temperature calculated at the end of the heat transfer analysis.

4.5. Investigation of frictional heating

Similarly, the impact of the frictional heat over the self–heating temperature can be investigated. Fig. 24 depicts the influence of applied strain on the maximum friction force in the delaminated region, and as a result, on the self-heating surface temperature. It can be observed that the temperature varies less than 0.3 ℃ for the strain range of interest. However, it is worth noting that Fig. 24 plots the maximum surface temperature as it would be capture by an IR camera.

The temperature at the crack tip is slightly higher as it is located two plies below the surface. This implies that components of different shapes should have distinct surface temperature distributions. For example, a thicker coupon may have a smaller increase in its surface hot-spot temperature, which may not be captured by an IR camera altogether.

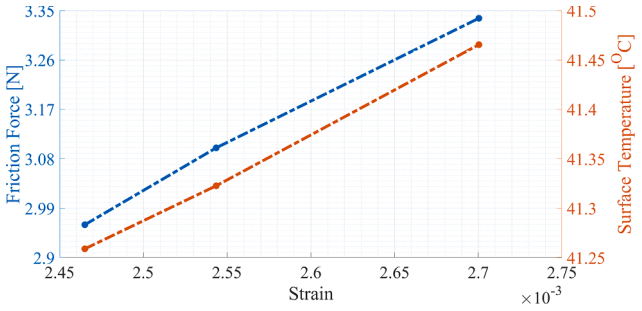

Fig. 24. The change in the Friction Force and its respective frictional Temperature due to the increase in the applied strain.

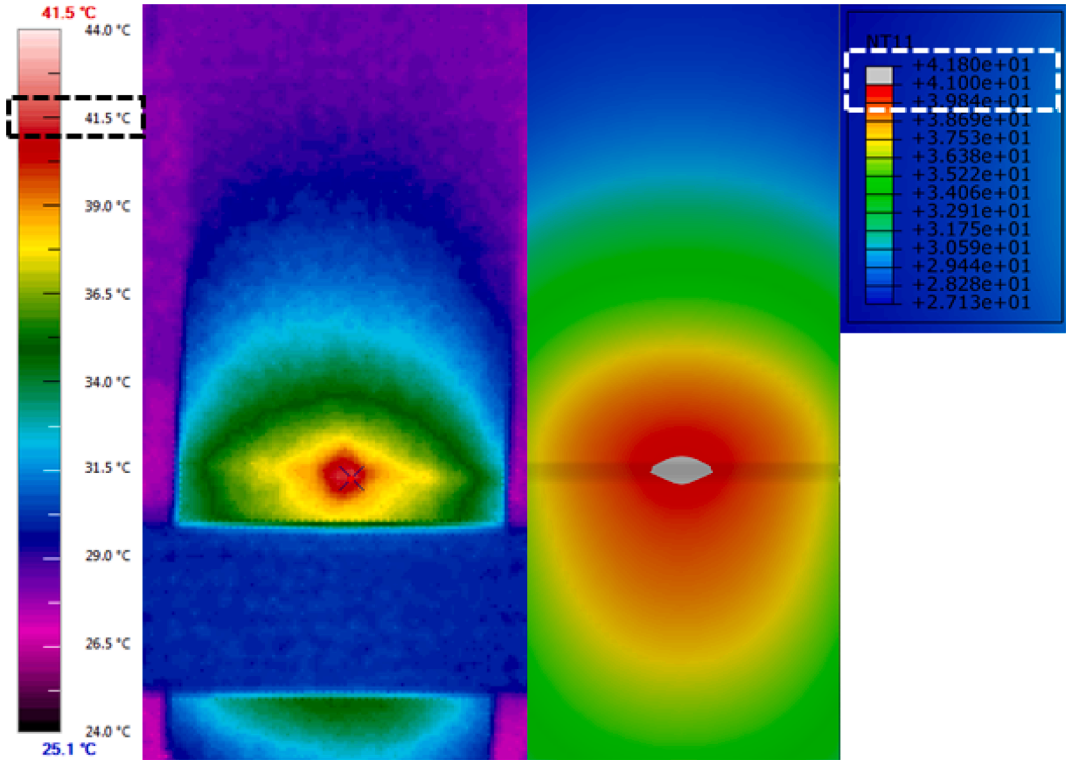

Fig. 23. Comparison between the experimental (top) and FE (bottom) Hot – Spot temperature distributions along the surface of a specimen / the Simulated Hot – Spot is depicted by the grey area.

In that sense, the FE model is able to capture information that can be challenging to observe experimentally.

The energy of the frictional heat can then be superimposed in order to simulate the hot-spot temperature. Fig. 25 shows the simulations of temperature distribution of the specimen due to the combined effect of frictional work and viscoelastic heat for two damage sizes (top and bottom). One can notice how the hot-spot size and temperature is enhanced as fatigue damage propagates. A delamination size even more significant than the one proposed by the final interrupted test was also introduced in the FE model to show that the model can also simulate the behaviour at the final stages of the fatigue life (when the test was interrupted).

5. Simulation of the relationship between the thermal and mechanical responses

This section will bring together both the VCCT analyses of the 2D model (section 3) and the heat transfer analyses of the 3D model (section 4). One might argue that such a combination might be questionable. Unfortunately, the VCCT for the 3D model was not achievable within the time frame of this research work. Therefore, combining both results aims to provide qualitative insights into the response and self-heating temperatures plotted against each other. Fig. 26 reports the simulation results for the thermal and mechanical responses at 25 ℃. This plot collates results from 2D and 3D models, where the phase drops with a higher magnitude than the measured one.

By repeating the process described in section 3 and 4 for different ambient temperatures, one could simulate relationships between response phases and self-heating temperatures as those measured and presented in Fig. 17. Fig. 27 shows those relationships for the experiments (in blue) and the simulations (red). Although the experimental relationships are linear fits of each ambient temperature presented in

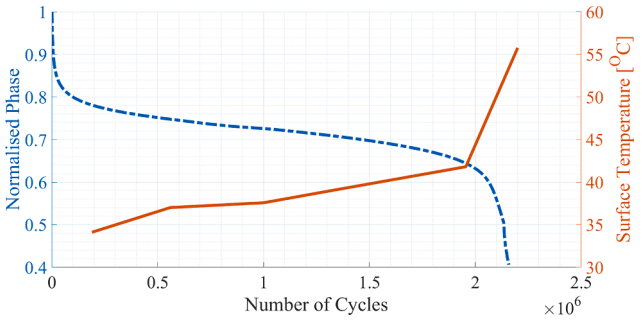

Fig. 26. Simulated Phase and Self – Heating Temperature Evolutions (based on the interrupted tests) at 25 ℃.

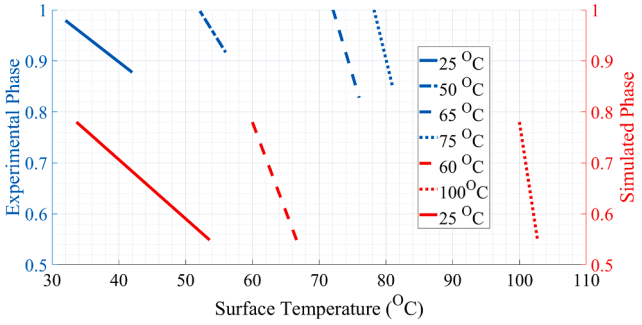

Fig. 27. A comparison between the Experimental and Simulated "Phase over Self-Heating Temperature" Curves.

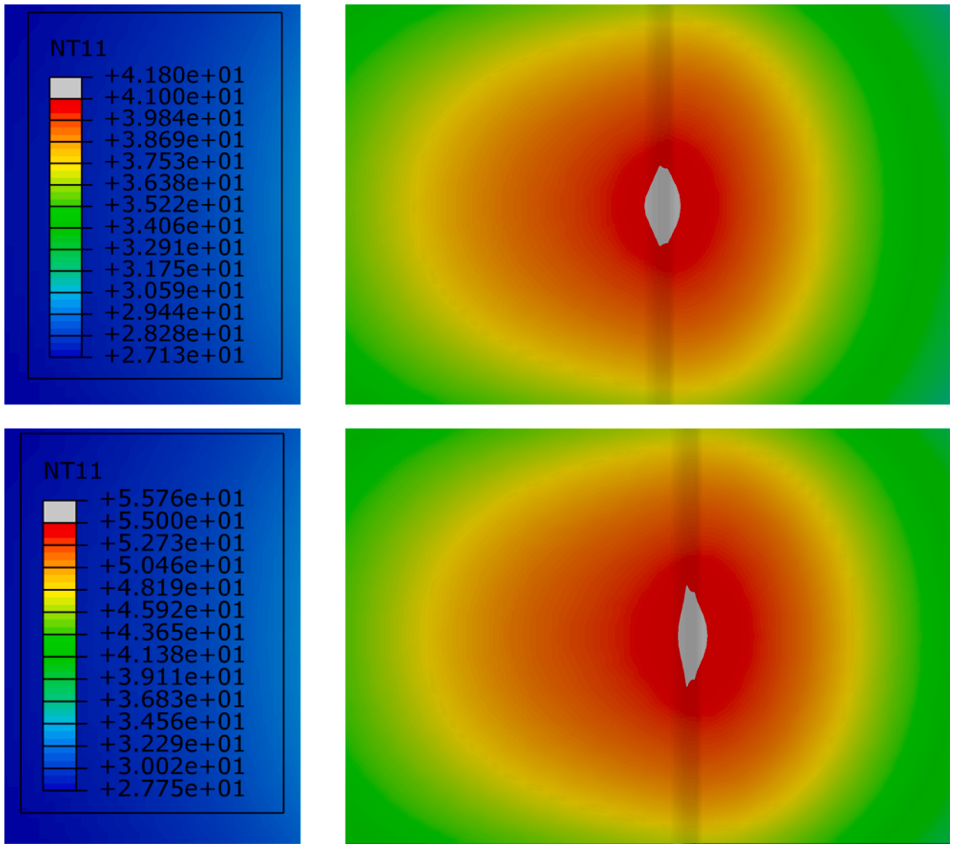

Fig. 25. The increase of the hot-spot temperature according the damage size; small damage top and large damage bottom.

Fig. 17, such a method avoided confusing the plot with redundant data.

-Is this thermo-mechanical model capable of simulating both the temperature offset caused by the ambient temperatures and the change of slopes caused by the self-heating behaviour of the phase-temperature relationships?

The answer is "yes!", and a further analysis carried out on the data plotted in Fig. 27 is presented in Fig. 28. The slopes, namely the "Rate of Change" of each phase-temperature relationship, were calculated from the experiments and the simulations. Fig. 28 shows the comparison between those slopes, which shows good agreement.

5.1. Simulation of cooling effect on delamination growth

Very briefly, this section will show how the simulation approach can be used for investigating how the cooling slows down fatigue.

In the main body of the text it was discussed how the strength of the VCCT model lies in revealing insights into high frequency testing in ways that are challenging to investigate experimentally. It is therefore logical to exploit this in order to study more complicated vibration fatigue behaviours. An experimental method has been described which was capable of delaying the Critical Event, under the application of different localised heat loads. The experimental data hinted that the extension in the fatigue life was the result of the suspension in the damage propagation rate.

It is however possible to simulate the experimental procedure by changing the specific temperature dependant parameters of the system. Actually, the simulation was initiated at 100 ℃, followed by a period during which the parameters were changed to simulate a 20 ℃ ambient temperature. After 1×10^5 cycles, the parameters adjusted back for 100 ℃ and the simulation was allowed to continue, normally. Fig. 29 presents a comparison between the phase responses when colling is applied given the same test severity. It can be confirmed what was suggested by the experimental analysis; that the growth rate is suspended during localised cooling. As a result, the fatigue life of the specimen is extended.

6. Discussions

This section will discuss the major outcomes of this research and the open questions.

The signature in the response phase trace, indicated as the Critical Event, is the result of mode-I failure, forcing the buckling of the surface ply, as shown in Fig. 11. Hence, the rate of delamination growth changes before and after the critical event because of the large forces at the crack tip separating the plies very rapidly. Another relevant outcome from the simulations, produced in Fig. 9, is the strain-independent behaviour of the delamination growth.

The authors declared that different material properties had to be used for the finite element model instead of the IM7/8552 used for the physical specimens. Arguably, this was quite a bold choice to overcome the limited materials data required for the complete spectrum analysis offered in this paper. Nonetheless, the results of the VCCT calculations,

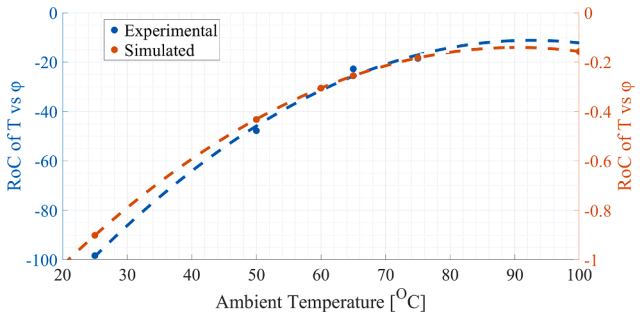

Fig. 28. Experimental and Simulated Rate of change of the "Self-Heating over Phase" curves.

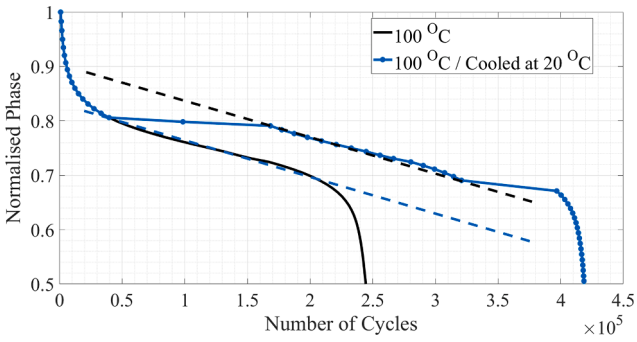

Fig. 29. Simulated Fatigue Damage Suspension Tests at the same ambient temperature and strain levels / Response Phase evolutions of the Cooled Test compared to original.

reproducing the response phase traces at various environmental temperature, showed a satisfactory agreement with the experimental ones (see Fig. 8 and Fig. 12). The S-N master curve generated by VCCT calculations and using the Critical Event's failure criterion, see Fig. 14_left, showed that the temperature created an offset (given the same strain load) but also showed that the physics of the self-heating were missed. In fact, the simulated S-N curves did not show the characteristic change of slope as visible in Fig. 14_right.

A relevant observation is the linear relationship between the delamination growth rate and the response phase decay rate, seen in Fig. 15. That linear relationship was already observed in [36] from the five interrupted tests, but the simulations remarked on linearity between damage growth and change in the response phase. Therefore, in future, one could calculate the damage growth rate from the measurement of response phase decay rate in real-time.

One shortcoming that needs to be pointed out is the performing of the VCCT analysis with a 2D model, which calculated the delamination as wide as the width of the specimen. This in return created a scaling factor such that the phase drop was more extensive than in experiments. Future work must exploit solid elements to avoid such discrepancy.

This paper also offers a detailed finite element analysis of the self-heating and frictional heating behaviour. Fig. 17 from [36] shows the experimental data when response phase and surface temperature traces are plotted against each other. One striking observation is that, given the error band of 5%, fewer tests would be needed to characterise the fatigue behaviour of the specimens. The multiphysics analyses could have been attempted by performing transient analysis or, as presented in this paper, by developing step-wise analyses which would allow constructing relationships between response phase, surface and environmental temperatures as the ones shown in Fig. 17.

The hysteretic self-heating can be simulated by simply calculating the modal strain energy; see region-A of Fig. 16. Experimental model validation can then be carried out to calibrate the final output of the temperature field, as seen in Fig. 19. The following region, indicated by region-B in Fig. 16, required to scale the modal strain energy using the calibration curve presented in Fig. 22. This process is a perfect example of the fusion of test and analysis where fewer experimental data (surface temperatures) are used to calibrate the numerical model. The final and most challenging part was to reconstruct the frictional heat produced by the delamination. In fact, the steady-state is linear analysis, whereas friction is a non-linear phenomenon. Transient was out of the question due to the extensive computational time required for solving the model. Hence, the transient behaviour of the temperature could be broken into steady-state analyses, which calculated the amount of work generated by the friction and scaled by the number of cycles. As a result, the temperature hot-spot could be reproduced for two steps.

Finally, Fig. 26 shows both the response phase simulations by 2D VCCT and surface temperature by 3D heat transfer analysis. By repeating the same process for different ambient temperatures, one could generate

the plot shown in Fig. 27 where both numerical and experimental data are compared. It is clear that the 2D VCCT overestimated the phase drops when compared to the experimental ones. Therefore, the slopes of both the simulated and experimental straight lines (response phase vs surface temperature) were collected and plotted in Fig. 28, showing the correctness of the simulations.

7. Conclusions

For the first time, the authors of this paper have shown how complex multiphysics experiments could be deconstructed into step-wise analyses by using finite element analysis. However, the paper never aspired to develop a predictive model. Actually, an intimate fusion of test and analysis approach was used to verify the objectives set at the beginning of the paper. Therefore, a simulation-driven dynamic testing could be used for investigating several characteristics of the fatigue behaviour of cross-ply laminate under vibration fatigue, which would otherwise be beyond the experimental capacity available in the proposed research.

Aside from the primary goals set and achieved throughout this research paper, the introduction discussed how self-heating could be a limiting factor when dealing with fatigue testing. This paper provides some guidance on how structural dynamics can be exploited for understanding those limiting factors very promptly and use those to enable more innovative mechanical tests.

Declaration of Competing Interest

The authors declare that they have no known competing financial interests or personal relationships that could have appeared to influence the work reported in this paper.

Acknowledgement

The authors wish to acknowledge EPSRC and Rolls-Royce plc. for supporting this research work.

References

[1] Alam P, Mamalis D, Robert C, Floreani C, Brádaigh CMÓ. The fatigue of carbon fibre reinforced plastics - A review. Compos. Part B Eng. 2019;166(February):555–79. https://doi.org/10.1016/j.compositesb.2019.02.016.
[2] Maquin F, Pierron F. Heat dissipation measurements in low stress cyclic loading of metallic materials: From internal friction to micro-plasticity. Mech. Mater. 2009;41(8):928–42.
[3] Guo Q, Zaïri F, Yang W. Evaluation of intrinsic dissipation based on self-heating effect in high-cycle metal fatigue. Int. J. Fatigue 2020;139:105653.
[4] Shen F, Kang G, Lam YC, Liu Y, Zhou K. Thermo-elastic-viscoplastic-damage model for self-heating and mechanical behavior of thermoplastic polymers. Int. J. Plast. 2019;121:227–43.
[5] Huang J, Garnier C, Pastor M-L, Gong X. Investigation of self-heating and life prediction in CFRP laminates under cyclic shear loading condition based on the infrared thermographic data. Eng. Fract. Mech. 2020;229:106971.
[6] Shojaei AK, Volgers P. Fatigue damage assessment of unfilled polymers including self-heating effects. Int. J. Fatigue 2017;100:367–76.
[7] Mahmoudi A, Mohammadi B. Theoretical-experimental investigation of temperature evolution in laminated composites due to fatigue loading. Compos. Struct. 2019;225:110972.
[8] Pitarresi G, Scalici T, Catalanotti G. Infrared Thermography assisted evaluation of static and fatigue Mode II fracture toughness in FRP composites. Compos. Struct. 2019;226:111220.
[9] Peyrac C, Jollivet T, Leray N, Lefebvre F, Westphal O, Gornet L. Self-heating method for fatigue limit determination on thermoplastic composites. Procedia Eng. 2015;133:129–35.
[10] Hülsbusch D, Kohl A, Striemann P, Niedermeier M, Strauch J, Walther F. Development of an energy-based approach for optimized frequency selection for fatigue testing on polymers–Exemplified on polyamide 6. Polym. Test. 2020;81:106260.
[11] Růžek R, Kadlec M, Petrusová L. Effect of fatigue loading rate on lifespan and temperature of tailored blank C/PPS thermoplastic composite. Int. J. Fatigue 2018;113(April):253–63. https://doi.org/10.1016/j.ijfatigue.2018.04.023.
[12] Lang RW, Manson JA. Crack tip heating in short-fibre composites under fatigue loading conditions. J. Mater. Sci. 1987;22(10):3576–80.
[13] Huang J, Li C, Liu W. Investigation of internal friction and fracture fatigue entropy of CFRP laminates with various stacking sequences subjected to fatigue loading. Thin-Walled Struct. 2020;155:106978.
[14] Mortazavian S, Fatemi A, Mellott SR, Khosrovaneh A. Effect of cycling frequency and self-heating on fatigue behavior of reinforced and unreinforced thermoplastic polymers. Polym. Eng. Sci. 2015;55(10):2355–67.
[15] Keoschkerjan R, Harutyunyan M, Wurmus H. Analysis of self-heating phenomenon of piezoelectric microcomponents actuated harmonically. Microsyst. Technol. 2003;9(1–2):75–80. https://doi.org/10.1007/s00542-002-0198-2.
[16] Katunin A, Hufenbach W. Frequency dependence of the self-heating effect in polymer-based composites. … Achiev. {…} 2010;41:9–15.
[17] Katunin A. Analytical model of the self-heating effect in polymeric laminated rectangular plates during bending harmonic loading. Maint. Reliab. 2010;4:91–101.
[18] Katunin A. Criticality of the self-heating effect in polymers and polymer matrix composites during fatigue, and their application in non-destructive testing. Polymers (Basel) 2019;11(1):19.
[19] Katunin A. Domination of self-heating effect during fatigue of polymeric composites. Procedia Struct. Integr. 2017;5:93–8.
[20] Katunin A. Evaluation of criticality of self-heating of polymer composites by estimating the heat dissipation rate. Mech. Compos. Mater. 2018;54(1):53–60.
[21] Katunin A, Wachla D. Analysis of defect detectability in polymeric composites using self-heating based vibrothermography. Compos. Struct. 2018;201:760–5.
[22] Katunin A, Wronkowicz A. Characterization of failure mechanisms of composite structures subjected to fatigue dominated by the self-heating effect. Compos. Struct. 2017;180:1–8.
[23] Katunin A. A concept of thermographic method for non-destructive testing of polymeric composite structures using self-heating effect. Sensors 2018;18(1):74.
[24] Katunin A, Fidali M. Fatigue and thermal failure of polymeric composites subjected to cyclic loading. Adv. Compos. Lett. 2012;21(3):63–9. https://doi.org/10.1177/096369351202100301.
[25] Katunin A. Critical self-heating temperature during fatigue of polymeric composites under cyclic loading. Compos. Theory Pract. 2012;1:72–6.
[26] Katunin A, Fidali M. Self-heating of polymeric laminated composite plates under the resonant vibrations: Theoretical and experimental study. Polym. Compos. 2012:138–46. https://doi.org/10.1002/pc.
[27] Katunin A, Wachla D. Minimizing self-heating based fatigue degradation in polymeric composites by air cooling. Procedia Struct Integrity 2019;vol. 18 (September):20–7. https://doi.org/10.1016/j.prostr.2019.08.136.
[28] Katunin A, Fidali M. Experimental identification of non-stationary self-heating characteristics of laminated composite plates under resonant vibration. Kompozyty 2011;3:214–9.
[29] a. Katunin, "Thermal fatigue of polymeric composites under repeated loading," *J. Reinf. Plast. Compos.*, vol. 31, no. 15, pp. 1037–1044, Aug. 2012, doi: 10.1177/0731684412452679.
[30] Katunin A, Wronkowicz A, Bilewicz M, Wachla D. Criticality of self-heating in degradation processes of polymeric composites subjected to cyclic loading: A multiphysical approach. Arch. Civ. Mech. Eng. 2017;17(4):806–15.
[31] Shou Z, Chen F, Yin H. Self-heating of a polymeric particulate composite under mechanical excitations. Mech. Mater. 2018;117:116–25.
[32] D. Di Maio and F. Magi, "Development of testing methods for endurance trials of composites components," *J. Compos. Mater.*, vol. 49, no. 24, 2015, doi: 10.1177/0021998314558497.
[33] Di Maio D, Magi F, Sever IA. Damage Monitoring of Composite Components under Vibration Fatigue using Scanning Laser Doppler Vibrometer. Exp. Mech. 2018;58(3):499–514. https://doi.org/10.1007/s11340-017-0367-y.
[34] Magi F, Di Maio D, Sever I. Damage initiation and structural degradation through resonance vibration: application to composite laminates in fatigue. Compos. Sci. Technol. 2016;132:47–56.
[35] Magi F, Di Maio D, Sever I. Validation of initial crack propagation under vibration fatigue by Finite Element analysis. Int. J. Fatigue 2017;104:183–94. https://doi.org/10.1016/j.ijfatigue.2017.07.003.
[36] Voudouris G, et al. Experimental fatigue behaviour of CFRP composites under vibration and thermal loading. Int. J. Fatigue 2020;vol. 140(May):105791. https://doi.org/10.1016/j.engfracmech.2019.106626.
[37] Khan B, Potter K, Wisnom MR. Suppression of delamination at ply drops in tapered composites by ply chamfering. J. Compos. Mater. 2006;40(2):157–74. https://doi.org/10.1177/0021998305053459.
[38] Agastra P, Mandell JF. Testing and simulation of damage growth at ply drops in wind turbine blade laminates. Int. SAMPE Symp. Exhib. 2010.
[39] Asp LE. The effects of moisture and temperature on the interlaminar delamination toughness of a carbon/epoxy composite. Compos. Sci. Technol. 1998;58(6):967–77.
[40] Sjögren A, Asp L, Greenhalgh E, Hiley M. Interlaminar Crack Propagation in CFRP: Effects of Temperature and Loading Conditions on Fracture Morphology and Toughness. Compos. Mater. Testing, Des. Accept. Criteria 2009. https://doi.org/10.1520/stp10643s.
[41] Sjögren A, Asp LE. Effects of temperature on delamination growth in a carbon/epoxy composite under fatigue loading. Int. J. Fatigue 2002;24(2–4):179–84. https://doi.org/10.1016/S0142-1123(01)00071-8.
[42] Russell AJ, Street KN. Predicting interlaminar fatigue crack growth rates in compressively loaded laminates. Compos. Mater. fatigue Fract. 1989:162–78.
[43] Matsubara G, Ono H, Tanaka K. Mode II fatigue crack growth from delamination in unidirectional tape and satin-woven fabric laminates of high strength GFRP. Int. J. Fatigue 2006;28(10):1177–86. https://doi.org/10.1016/j.ijfatigue.2006.02.006.

[44] Bolotin VV. Delaminations in composite structures: its origin, buckling, growth and stability. Compos. Part B Eng. 1996;27(2):129–45.
[45] F. Lahuerta, T. Westphal, and R. P. L. Nijssen, "Self-heating forecasting for thick laminates testing coupons in fatigue".
[46] C. Fiber, "HexTow ® IMA IM7 Datasheet," vol. 000, pp. 1–2, 2016.
[47] Saad MT, Miller SG, Marunda T. THERMAL CHARACTERIZATION OF IM7/8552-1 CARBON-EPOXY COMPOSITES. In: *Proceedings of the ASME 2014 International Mechanical Engineering Congress and Exposition*; 2014. p. 1–8.
[48] Furkan Ismail Ulu. Measurement of Multidirectional Thermal Conductivity of IM7-G/8552 Unidirectional Composite Laminate. North Carolina A&T: State University; 2015.
[49] Schön J. Coefficient of friction and wear of a carbon fiber epoxy matrix composite. Wear 2004;257(3–4):395–407. https://doi.org/10.1016/j.wear.2004.01.008.